Aalborg Universitet

AALBORG UNIVERSITY

An Enhanced Power Sharing Scheme for Voltage unbalance and harmonics compensation in an islanded AC microgrid

Han, Yang; Shen, Pan; Zhao, Xin; Guerrero, Josep M.

An Enhanced Power Sharing Scheme for Voltage Unbalance and Harmonics Compensation in an Islanded AC Microgrid

Yang Han, *Member, IEEE*, Pan Shen, Xin Zhao, and Josep M. Guerrero, *Fellow, IEEE*

Abstract—In this paper, an enhanced hierarchical control structure with multiple current loop damping schemes for voltage unbalance and harmonics compensation in ac islanded microgrid is proposed to address unequal power sharing problems. The distributed generation (DG) is properly controlled to autonomously compensate voltage unbalance and harmonics while sharing the compensation effort for the real power, reactive power, unbalance and harmonic powers. The proposed control system of the microgrid mainly consists of the positive sequence real and reactive power droop controllers, voltage and current controllers, the selective virtual impedance loop, the unbalance and harmonics compensators, the secondary control for voltage amplitude and frequency restoration, and the auxiliary control to achieve a high voltage quality at the point of common coupling (PCC). By using the proposed unbalance and harmonics compensation (UHC), the auxiliary control, and the virtual positive/negative-sequence impedance (VPI/VNI) loops at fundamental frequency, and the virtual variable harmonic impedance (VVHI) loop at harmonic frequencies, an accurate power sharing is achieved. Moreover, the low bandwidth communication (LBC) technique is adopted to send the compensation command of the secondary control and auxiliary control from the microgrid control center (MGCC) to the local controllers of DG unit. Finally, the hardware-in-the-loop (HIL) results using dSPACE 1006 platform are presented to demonstrate the effectiveness of the proposed approach.

Index Terms—Distributed generation, microgrid, droop control, voltage unbalance and harmonics compensation, power sharing, virtual impedance, secondary control, auxiliary control.

Y. Han and P. Shen are with the Department of Power Electronics, School of Mechatronics Engineering, University of Electronic Science and Technology of China, No.2006, Xiyuan Avenue, West Hi-Tech Zone, Chengdu 611731, China (e-mail: hanyang@uestc.edu.cn; panshen01@126.com).

X. Zhao and J. M. Guerrero are with the Department of Energy Technology, Aalborg University, 9220 Aalborg East, Denmark (e-mail: joz@et.aau.dk).

NOMENCLATURE

Abbreviations

DG	Distributed generation.
RES	Renewable energy resource.
APF	Active power filter.
VSI	Voltage source inverter.
PCC	Point of common coupling.
ESS	Energy storage system.
PV	Photovoltaic cell.
SoC	State of charge.
EMU	Energy management unit.
DSC-SOGI	Delayed-signal cancellation with second order generalized integrator.
VPI	Virtual positive-sequence impedance.
VNI	Virtual negative-sequence impedance.
VVHI	Virtual variable harmonic impedance.
UHC	Unbalance and harmonic frequencies.
LBC	Low bandwidth communication.
HIL	Hardware-in-the-loop.
MGCC	Microgrid control center.
SISO	Single input single output.
P+MRC	Proportional plus multi-resonant controllers.
LPF	Low pass filter.
PI	Proportional integral.
SW	Switch.

Variables

i_{Labc}	Inverter currents.
i_{oabc}	Output currents.
v_{oabc}	Output voltages.
i_α, i_β	Current components in $\alpha\beta$-axis.
v_α, v_β	Voltage components in $\alpha\beta$-axis.
v_{dc}	Voltage at dc side of the VSI.
p, q	Instantaneous real and reactive powers.
P^+, Q^+	Positive-sequence real and reactive powers at fundamental frequency.
D	Harmonic power.
Q_N	Unbalance power.
$i_{o\alpha,f}^+, i_{o\beta,f}^+$	Fundamental positive-sequence output current.
$i_{o\alpha,f}^-, i_{o\beta,f}^-$	Fundamental negative-sequence output current.
$i_{o\alpha,h}^h, i_{o\beta,h}^h$	Sequence component of hth harmonic currents.
$v_{o\alpha\beta,f}^-$	Fundamental negative-sequence output voltage.

$v_{o\alpha\beta,h}^{\pm}$	Sequence component of hth harmonic voltages.
$Z_{v\alpha\beta}$	Resistive-inductive virtual impedance.
$Z_{o\alpha\beta}$	Output impedance.
ω, E	Angular frequency and amplitude of the output voltage reference.
ω_{MG}, E_{MG}	Angular frequency and voltage amplitude of the islanded microgrid.
K_{UHCR}	Output signal of unbalance and harmonics compensation block.
$C_{\alpha\beta}^{h\pm}$	Compensation reference of each harmonic.
$C_{\alpha\beta}^{*}$	Output signal of the auxiliary controller.
$D_{dq}^{h\pm}$	The hth harmonic compensation for the PCC voltage in dq frame.

Parameters

ω_{LPF}	Cut-off frequency of the LPF.
v^{*}	Rated phase voltage.
P^{+*}, Q^{+*}	Fundamental positive-sequence real and reactive power references.
$R_{v,f}^{\pm}, L_{v,f}^{\pm}$	Virtual fundamental-frequency positive- and negative-sequence resistive and inductance.
$R_{v,h}, L_{v,h}$	Virtual harmonic-frequency resistance and inductance.
K_N, K_H	Coefficients of the unbalance and harmonics compensator.
T_s	Sampling time.
k_{pf}, k_{if}	Parameters of the frequency restoration control.
k_{pe}, k_{ie}	Parameters of the voltage restoration control.
$\omega_{MG}^{*}, E_{MG}^{*}$	Angular frequency and voltage amplitude references of the islanded microgrid.
τ	PLL time constant.
k_p, k_q	Frequency and voltage droop coefficients.
ω_0	Fundamental frequency.
$CG_{h\pm}$	Compensation gain for the hth voltage harmonic.
$HD_{I,h\pm}$	Distortion index of hth harmonic current.
$HD_{I,h\pm}^{max}$	Maximum h^{th} harmonic current distortion index.
$S_{0,j}$	Nominal power of the jth DG.
L_{DG}, R_{DG}	DG feeder inductance and resistance.
L, L_o	Filter and output inductances.
C	Filter capacitance.
L_{NL}, R_{NL}, C_{NL}	Nonlinear load parameters.
R_{UL}	Unbalanced load resistance.
R_{BL}	Balanced load resistance.
ω_c	Cut-off frequency of the voltage controller.
k_{pv}, k_{rv}, k_{hv}	Parameters of the voltage controller.
k_c	Proportional value of the current controller.

I. INTRODUCTION

Distributed generation (DG) using renewable energy resource (RES) such as wind turbines and solar power plants has been widely used in recent years. However, the increasing penetration of the DG systems may bring problems like inverse power flow, voltage deviation, and voltage fluctuation to the distribution networks [1]. To achieve better operation of multiple DG units, the microgrid concept using the coordinated control strategies among parallel-connected DG interfacing converters has been presented [2-5].

Compared to the conventional distribution system, the microgrid can operate in both grid-connected and autonomous islanding modes, offering more reliable power to the critical loads. In the islanded mode, each DG unit should be able to supply certain amount of the total load proportional to its power rating. To achieve the power sharing requirement with only local measurement and eliminating an external high bandwidth communication links among the DG units, the frequency and voltage droop control methods are widely adopted [3-10] and the "plug-and-play" interfacing functions can be applied to enhance the reliability of the system [11]. However, the conventional droop control method has several drawbacks including a trade-off between power sharing accuracy and voltage deviation, unbalanced harmonic current sharing and a high dependency on the line impedances [12]. Although the accurate real power sharing can be achieved by the frequency droop method, the poor reactive power sharing due to impedance mismatch of the DG feeders and the different ratings of the DG units is inevitable [6]. To cope with these drawbacks, the modified droop control methods using virtual frequency-voltage frame or virtual real and reactive power concept are proposed [13], [14]. However, the accuracy of reactive power sharing is difficult to be improved by using the modified droop control methods. In addition, the virtual impedance aided DG operation is considered to be a promising way to enhance the performance of the microgrid, but the main focus is the behavior of virtual impedance at fundamental frequency as discussed in [3], [5], [15-18].

It is well known that the primary control, which contains droop control, voltage and current controllers and virtual impedance loop, does not require high bandwidth communication, and the secondary control is often adopted in order to achieve global controllability of the microgrid [16]. The secondary control is presented to compensate the deviations of the voltage and frequency inside the microgrid [12], [16]. Furthermore, the global objectives regarding voltage control and power quality of the microgrid, such as voltage unbalance and harmonic compensation have been discussed in additional secondary control loops [19], [20].

Note that the proliferation of unbalanced and nonlinear loads in the distribution networks results in various power quality problems for microgrids since it lacks the voltage and frequency support from the utility [15], [21-24]. Therefore, a microgrid should be able to operate under unbalanced and nonlinear load conditions without performance degradations. In order to overcome the power quality problems, the series active power filters (APFs) can be utilized to compensate the voltage unbalance and harmonics by injecting negative sequence and harmonic voltage to the distribution line through coupling transformers [25], [26]. However, installation of the extra APFs for each of the DGs is costly for the islanded microgrid conditions. On the other hand, the voltage unbalance and harmonics compensation capability can be achieved by proper control of the voltage source inverters (VSIs) [15], [17], [21-23], [27]. In [17], the unbalanced voltage of the microgrid is compensated under unbalanced load conditions. However, the unbalanced voltage drop across the virtual impedance is not considered, which leads to a limited performance for the unbalance compensation of the output voltage. In [25], the harmonic and negative-sequence currents are compensated under nonlinear and unbalanced load conditions. However, the

droop control without considering the positive sequence real and reactive powers and the power sharing is inaccurate. In addition, the virtual impedance loop is developed to adjust DG equivalent impedance at fundamental positive and negative sequences and harmonic frequencies to alleviate the circulating currents and unbalanced and harmonic power sharing problems [22], [23]. Moreover, the harmonic compensation methods are designed for compensation of voltage harmonics at the DG terminal while the power quality at the point of common coupling (PCC) is the main concern due to the sensitive loads [28]. Thus, a good power quality can be guaranteed for the sensitive loads connected to PCC by compensation of PCC voltage harmonics.

Most of the existing works on the control and power management for islanded microgrids [6], [15-17], [22], [29-34], where the power sharing problems with the mismatched feeder impedance and the power quality problems under the unbalanced and nonlinear loads are seldom fully considered. In [22], an enhanced droop control method through online virtual impedance adjustment is proposed to address inaccurate power sharing problems, but the time varying soft compensation factor is difficult to be calculated. An autonomous active power control to coordinate the distributed components of microgrid consisting of the energy storage system (ESS), the photovoltaic (PV) systems, and loads is analyzed in [29], which keeps the state of charge (SoC) of the ESS within the safe limits by automatically adjusting the power generation from the PV systems and load consumption. In [30], an estimator-based voltage-predictive control strategy for ac islanded microgrids is presented to perform voltage control without communication facilities. However, the power management and the nonlinear and unbalanced loads are not taken into account. Moreover, a networked-based hybrid distributed structure of the control strategy that enables optimized operation of the microgrid systems based on the operational objectives decided by the energy management unit (EMU) is presented in [31], which eliminates the reactive power sharing errors associated with the conventional droop control without compromising system stability. Taking into account the control modes and configurations of a microgrid, the proper power sharing among DGs can be ensured by modifying the droop constants of the feeder flow control mode of the DG units [32]. In addition, an improved droop control method for reactive power sharing is presented in [33]. The sharing accuracy is improved by the sharing error reduction operation and the voltage recovery operation is used to compensate the decrease caused by the error reduction operation. To avoid the complex power management algorithms, the converter parameters are adopted as apparent power limit and maximum active power to manage reactive power sharing in the hierarchical control structure [34].

In this paper, an enhanced hierarchical control methodology is applied to DG units in an islanded microgrid. The selective virtual impedance at the fundamental positive sequence, fundamental negative sequence, and harmonic frequencies are adopted to achieve better power sharing of reactive, unbalance and harmonic powers. The delayed-signal cancellation with second order generalized integrator (DSC-SOGI)-based sequence decomposition is used to extract the fundamental positive- and negative-sequence currents, and the harmonic components, which is composed of the virtual positive/

negative-sequence impedance (VPI/VNI) loops at fundamental frequency, and the virtual variable harmonic impedance (VVHI) loop at harmonic frequencies. The VPI and VNI loops at fundamental frequency improve the performance of the real power frequency (P-ω) and reactive power-voltage magnitude (Q-E) droop controllers and reduce the fundamental negative sequence circulating currents. In addition, a proper sharing of harmonic power among all the DG inverters is achieved by using the VVHI loop at the characteristic harmonic frequencies.

Furthermore, an unbalance and harmonics compensation (UHC) is proposed to change of the voltage reference to compensate for voltage unbalance and harmonic in a microgrid. The centralized secondary control scheme for voltage amplitude and frequency restoration purposes of microgrid and the auxiliary controller of selective harmonics compensation of the PCC main voltage harmonics with the low bandwidth communication (LBC) link are also presented in this paper. It is a practical and cost-effective approach since only a LBC network is required. The feasibility of the proposed approach is validated by the hardware-in-the-loop (HIL) results obtained from the two parallel-connected inverters under balanced and unbalanced resistive loads and/or nonlinear load conditions using dSPACE 1006 platform. The main contributions of this paper are summarized as follows.

1) Development of an enhanced hierarchical power sharing method for an islanding microgrid under nonlinear and/or unbalanced load conditions. The UHC module is proposed to compensate for voltage unbalanced and harmonics in a microgrid.

2) Implementation of the VPI and VNI loops at fundamental frequency, and the VVHI loop at harmonic frequencies to compensate the reactive, unbalance and harmonic power sharing errors. The DSC-SOGI-based sequence decomposition method is adopted for the accurate load current decomposition and reference current generation.

3) Implementation of combined the primary, secondary and auxiliary control approaches to improve the power quality of the PCC voltage and power sharing accuracy.

The rest of this paper is organized as follows. The decentralized microgrid system configuration is constructed in Section II. The dynamic model of a DG unit is presented in Section III. The proposed hierarchical control strategy of the islanded microgrid system is analyzed in detail in Section IV, including the primary control, secondary control, and the auxiliary control. Moreover, the hardware-in-the-loop (HIL) test results using dSPACE 1006 platform are presented to demonstrate the validity and effectiveness of the proposed control strategy in Section V. Finally, the main conclusion and contributions of this paper are highlighted in Section VI.

II. DECENTRALIZED MICROGRID SYSTEM CONFIGURATION

A typical system configuration of a low-voltage microgrid with n DG units and complex load conditions is given in Fig. 1. For each DG unit, the dc power is provided by the RES, and an ideal dc-link with fixed dc voltage is assumed in this paper to simplify the theoretic analysis. The DG units are integrated to the microgrid with LCL filters, and each DG unit is connected to the PCC through a distortion feeder. Moreover, there are a few unbalanced and harmonic loads connected at the PCC.
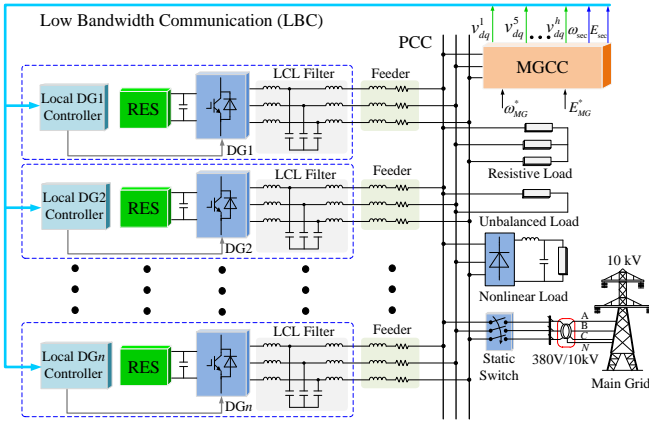
Fig. 1. Typical structure of MG with multiple parallel-connected DG units.

In addition, the individual components of PCC voltage harmonics are extracted and sent to all DG units. The LBC is applied for sending the data information of the secondary controllers and the PCC voltage harmonics from the microgrid control center (MGCC) to the local controller to realize the proposed compensation scheme in DG units in a practical and synchronized manner. Furthermore, a static switch is used to dynamically disconnect the microgrid from the upstream distribution system in case of grid faults. Although the proposed control strategies can operate in either the grid-connected mode or islanded mode, only the islanded operation mode will be considered in this paper.

III. DYNAMIC MODEL OF A DG UNIT

The power stage of a DG unit and the proposed hierarchical control strategy for the interface inverter connected in an islanded mode is shown in Fig. 2. The DG unit with its LCL filter can be considered as a subsystem of the microgrid. In this section, the dynamic model of a DG unit, as a subsystem of the overall microgrid, is presented. The circuit diagram of DG i is used as an illustration to construct the dynamic model.

The objective is to design a feedback control system to regulate output voltage of each DG and load voltages in the presence of load disturbances. Notably, each DG unit is a three-phase three-wire system, thus the zero-sequence currents become zero. By using *Kirchhoff's Voltage Law* and *Kirchhoff's Current Law* [35], LC output filter shown in Fig. 2 yields the following differential equations

$$\begin{cases} \boldsymbol{T}_T \dfrac{d\boldsymbol{I}_L}{dt} = \dfrac{1}{L}\boldsymbol{V} - \dfrac{1}{L}\boldsymbol{T}_T\boldsymbol{V}_o \\ C\dfrac{d\boldsymbol{V}_o}{dt} = \boldsymbol{I}_C = \boldsymbol{I}_L - \boldsymbol{I}_o \end{cases}, \quad \boldsymbol{T}_T = \begin{bmatrix} 1 & -1 & 0 \\ 0 & 1 & -1 \\ -1 & 0 & 1 \end{bmatrix} \quad (1)$$

where $\boldsymbol{V}=[v_{ab}, v_{bc}, v_{ca}]^T$ is the inverter output line to line voltage vector, $\boldsymbol{I}_L=[i_{La}, i_{Lb}, i_{Lc}]^T$ is the inverter phase current vector, $\boldsymbol{I}_o=[i_{oa}, i_{ob}, i_{oc}]^T$ is the load phase current vector, $\boldsymbol{I}_C=[i_{Ca}, i_{Cb}, i_{Cc}]^T$ is the capacitor current vector, $\boldsymbol{V}_o=[v_{oa}, v_{ob}, v_{oc}]^T$ is the line to neutral voltage vector at the load side.

The Clarke transformation is adopted to transform the variables between *abc* and *αβ* frames. The state-space equation of the system in the *αβ* frame is obtained as follows [24], [36]

$$\dot{x}_s = \mathbf{A}_s x_s + \mathbf{B}_s u_s + \mathbf{D}_s w_s, \quad y_s = \mathbf{F}x_s \quad (2)$$

where $x_s=[v_{o\alpha}, v_{o\beta}, i_{L\alpha}, i_{L\beta}]^T$, $u_s=[v_\alpha, v_\beta]^T$, $w_s=[i_{o\alpha}, i_{o\beta}]^T$, $y_s=[v_{o\alpha},$

$v_{o\beta}]^T$, and the matrices $\mathbf{A}_s$, $\mathbf{B}_s$, $\mathbf{D}_s$ and $\mathbf{F}$ are

$$\mathbf{A}_s = \begin{bmatrix} 0 & 0 & 1/C & 0 \\ 0 & 0 & 0 & 1/C \\ -1/L & 0 & 0 & 0 \\ 0 & -1/L & 0 & 0 \end{bmatrix}, \quad \mathbf{B}_s = \begin{bmatrix} 0 & 0 \\ 0 & 0 \\ 1/L & 0 \\ 0 & 1/L \end{bmatrix},$$

$$\mathbf{D}_s = \begin{bmatrix} -1/C & 0 \\ 0 & -1/C \\ 0 & 0 \\ 0 & 0 \end{bmatrix}, \quad \mathbf{F} = \begin{bmatrix} 1 & 0 & 0 & 0 \\ 0 & 1 & 0 & 0 \end{bmatrix}. \quad (3)$$

Equation (2) can be rewritten in the Laplace domain as

$$v_{o\alpha\beta}(s) = \begin{bmatrix} \dfrac{1}{LCs^2+1} & 0 \\ 0 & \dfrac{1}{LCs^2+1} \end{bmatrix} v_{\alpha\beta}(s) - \begin{bmatrix} \dfrac{Ls}{LCs^2+1} & 0 \\ 0 & \dfrac{Ls}{LCs^2+1} \end{bmatrix} i_{o\alpha\beta}(s)$$

$$(4)$$

Equation (4) shows that the matrix transfer function of the DG subsystem is diagonal (completely decoupled) and can be viewed as two single input single output (SISO) control system, which facilitates the forthcoming controller design procedure.

IV. PROPOSED HIERARCHICAL CONTROL STRATEGY

As shown in Fig. 2, the error signals obtained by comparing the measured output voltage, the voltage drop generated by the selective virtual impedance loop, the power controllers, the selective harmonics compensation of PCC, the UHC block, and the reference value which are regulated by the proportional plus multi-resonant controllers (P+MRC) to generate references for the current loop. The reference current signals are then compared with the corresponding inverter currents, and are regulated by a proportional controller to produce voltage commands. Moreover, in order to activate the compensation strategy in multiple parallel-connected DG units synchronously, the LBC bus is used to send the compensation command from the MGCC to the local DG controller, including the secondary control and auxiliary control. The proposed hierarchical control strategies are presented as follows.

A. The Primary Control

A.1. Power Droop Control Loop

The three-phase instantaneous real power (p) and reactive power (q) are calculated from $\alpha\beta$-axis output voltage ($v_{C\alpha\beta}$) and output current ($i_{o\alpha\beta}$) as

$$p = v_{o\alpha}i_{o\alpha} + v_{o\beta}i_{o\beta} \quad (5)$$

$$q = v_{o\beta}i_{o\alpha} - v_{o\alpha}i_{o\beta} \quad (6)$$

Each of the instantaneous powers calculated using (5) and (6) consists of dc and ac components. The ac parts are fundamental positive-sequence active and reactive powers that can be extracted using low pass filters (LPFs). The ac parts are generated by the unbalance and harmonic components of the output voltages and currents.

In order to extract the fundamental positive sequence and negative sequence currents as well as the dominant harmonic currents, the DSC-SOGI based sequence decomposition is used to extract the fundamental positive, negative and harmonic components of the output currents [37]. A simplified detection
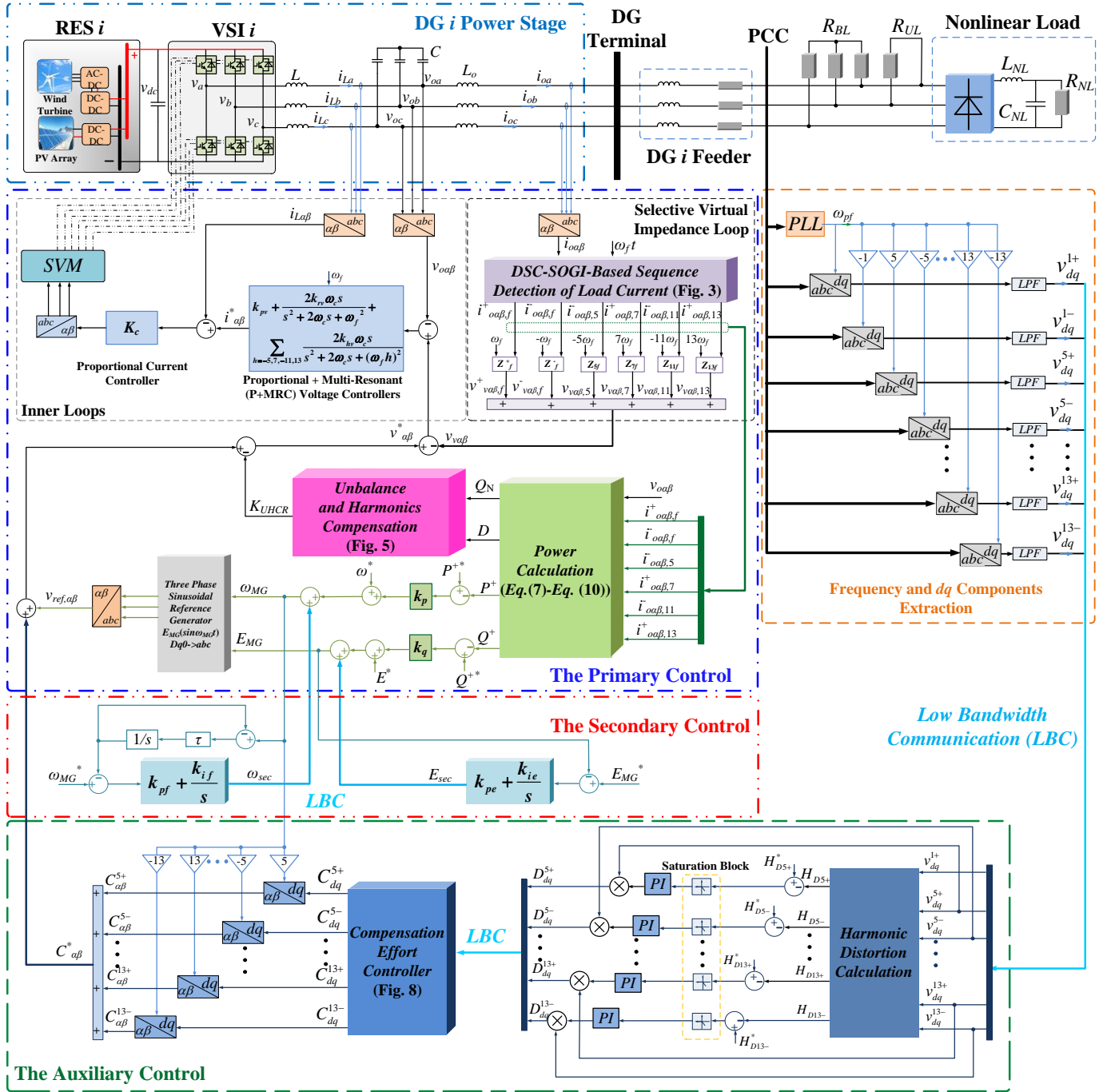
Fig. 2. Block diagram of the proposed hierarchical control strategy for the islanded microgrid.

diagram of the DSC-SOGI based sequence decomposition is depicted in Fig. 3. With the detected current components, the instantaneous powers of a three-phase DG unit are then passed through LPFs with 2 Hz cut-off frequency (ω_{LPF}) to obtain the filtered output real and reactive powers, harmonic and negative powers as follows [38]

$$P^+ = \left[\omega_{LPF} / (s + \omega_{LPF})\right](v_{o\alpha} i^+_{o\alpha,f} + v_{o\beta} i^+_{o\beta,f}) \tag{7}$$

$$Q^+ = \left[\omega_{LPF} / (s + \omega_{LPF})\right](v_{o\beta} i^+_{o\alpha,f} - v_{o\alpha} i^+_{o\beta,f}) \tag{8}$$

$$D = v^* \sqrt{\begin{array}{l}(i^-_{o\alpha,5})^2 + (i^-_{o\beta,5})^2 + (i^+_{o\alpha,7})^2 + (i^+_{o\beta,7})^2 + \\ (i^-_{o\alpha,11})^2 + (i^-_{o\beta,11})^2 + (i^+_{o\alpha,13})^2 + (i^+_{o\beta,13})^2\end{array}} \tag{9}$$

$$Q_N = v^* \sqrt{(i^-_{o\alpha,f})^2 + (i^-_{o\beta,f})^2} \tag{10}$$

where P^+ and Q^+ are the real and reactive powers, respectively. The ripples in real and reactive power are attenuated by using the LPFs. Note that the bandwidth of the LPF is much smaller than that of inner controllers of DG unit and the performance of the system is strongly influenced by this fact [39]. Moreover, only dominate low order harmonic currents are adopted to calculate the harmonic power. The variables D and Q_N are harmonic power and unbalance power, respectively, v^* is the rated phase voltage, $i^+_{o\alpha,f}$ and $i^+_{o\beta,f}$ are fundamental positive-sequence output current, $i^-_{o\alpha,f}$ and $i^-_{o\beta,f}$ are fundamental negative-sequence output current, $i^h_{o\alpha,h}$ and $i^h_{o\beta,h}$ are the sequence

component of hth harmonic currents and h denotes the dominant harmonic components (h=-5, 7, -11, 13, etc.).
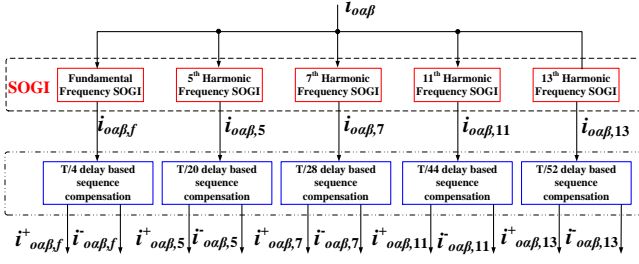
Fig. 3. The DSC-SOGI based sequence decomposition of fundamental positive sequence, fundamental negative sequence, and harmonic components.

At a local DG unit controller, the droop control is utilized to avoid communication wires while obtaining good power sharing, which is responsible for adjusting the frequency and amplitude of the voltage reference according to the positive sequence real and reactive powers (P^+ and Q^+), ensuring P^+ and Q^+ flow control [16], [18]. The positive sequence real power-frequency (P^+-ω) and reactive power-voltage magnitude (Q^+-E) droop controllers are defined as

$$\omega = \omega^* - k_p(P^+ - P^{+*}) \quad (11)$$

$$E = E^* - k_q(Q^+ - Q^{+*}) \quad (12)$$

where ω and E represent the frequency and amplitude of the output voltage reference, ω^* and E^* are the nominal frequency and amplitude, P^+* and Q^+* are the fundamental positive-sequence real and reactive power references normally set to zero in islanded microgrid, and k_p and k_q are droop coefficients.

A.2. DSC-SOGI Based Selective Virtual Impedance Loop

Virtual resistance enhances system damping without adding additional power loss, since it is realized by a control loop and it is possible to implement without decreasing system efficiency. Moreover, the virtual inductance is utilized to make the DG output impedance more inductive to improve decoupling of P and Q, thus enhances the system stability, and reduces power oscillations and circulating currents [3], [18]. As shown in Fig. 4, the voltage drop across the VPI, VNI and VVHI loops in $\alpha\beta$ reference frame are

VPI loop:
$$\begin{bmatrix} v_{v\alpha,f}^+ \\ v_{v\beta,f}^+ \end{bmatrix} = \begin{bmatrix} R_{v,f}^+ & -\omega_f L_{v,f}^+ \\ \omega_f L_{v,f}^+ & R_{v,f}^+ \end{bmatrix} \begin{bmatrix} i_{o\alpha,f}^+ \\ i_{o\beta,f}^+ \end{bmatrix} \quad (13)$$

VNI loop:
$$\begin{bmatrix} v_{v\alpha,f}^- \\ v_{v\beta,f}^- \end{bmatrix} = \begin{bmatrix} R_{v,f}^- & \omega_f L_{v,f}^- \\ -\omega_f L_{v,f}^- & R_{v,f}^- \end{bmatrix} \begin{bmatrix} i_{o\alpha,f}^- \\ i_{o\beta,f}^- \end{bmatrix} \quad (14)$$

VVHI loop:
$$\begin{bmatrix} v_{v\alpha,h} \\ v_{v\beta,h} \end{bmatrix} = \begin{bmatrix} R_{v,h} & h\omega_f L_{v,h} \\ R_{v,h} & -h\omega_f L_{v,h} \end{bmatrix} \begin{bmatrix} i_{o\alpha,h}^h \\ i_{o\beta,h}^h \end{bmatrix} \quad (15)$$

where $v_{v\alpha\beta,f}^+$ and $v_{v\alpha\beta,f}^-$ represent the virtual fundamental-frequency positive- and negative-sequence voltage drops, $v_{v\alpha\beta,h}$ is the virtual harmonic-frequency voltage drop, $R_{v,f}^+$ and $L_{v,f}^+$ are the virtual fundamental-frequency positive-sequence resistance and inductance, $R_{v,f}^-$ and $L_{v,f}^-$ represent the virtual fundamental-frequency negative-sequence resistance and inductance, $R_{v,h}$ and $L_{v,h}$ represent the virtual harmonic-frequency resistance and inductance, and h denotes the dominant harmonic components (h=-5, 7, -11, 13, etc.), and ω_f represents the system fundamental frequency.
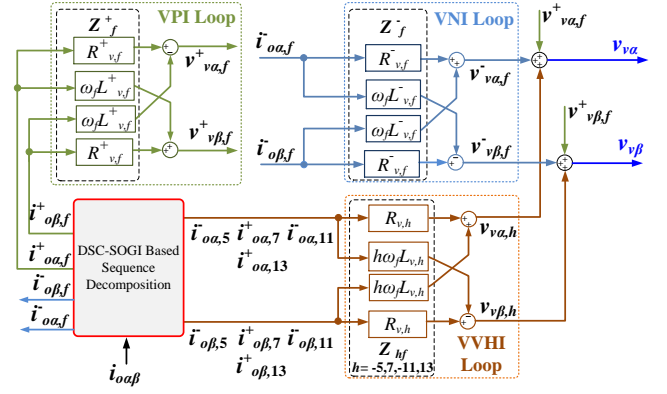
Fig. 4. Block diagram of DSC-SOGI-based selective virtual impedance loop.

At the fundamental frequency, the VPI loop is designed to be inductive to improve the reactive power sharing based on the Q^+-E droop. In addition, the VNI is designed to be resistive to minimize the undesired negative sequence circulating currents among the DG units [23]. Furthermore, the size of negative inductance needs to be kept smaller than the effective inductance to guarantee the stability of the VVHI loop at harmonic frequencies, and the better harmonic power sharing can be achieved by using a larger positive resistance in the VVHI loop [22], [23], [40].

A.3. Local Unbalance and Harmonics Compensation Scheme

It is well known that voltage unbalance and harmonics leads to the appearance of the negative sequence and harmonic components [15], [19], [21-25], [27]. Thus, the compensation of the voltage unbalance and harmonics can be achieved by reducing the negative sequence and harmonics voltages. As shown in Fig. 2, the output of the unbalance and harmonics compensation (UHC) block [unbalance and harmonics compensation reference (K_{UHCR})] is injected as a reference for the voltage controller.
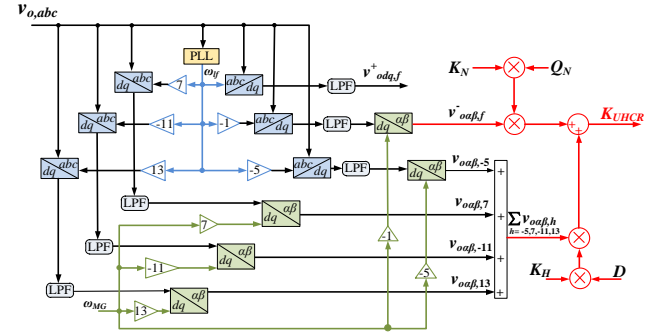
Fig. 5. Block diagram of the local unbalance and harmonics compensation.

As shown in Fig. 5, the fundamental negative sequence reactive power (Q_N) and the fundamental harmonic components reactive power (D) are multiplied by two constant values (K_N and K_H), and also by the instantaneous fundamental negative sequence voltage ($v_{o\alpha\beta,f}^-$) and the total harmonics voltage ($\sum v_{o\alpha\beta,h}$) to generate this compensation reference, then the K_{UHCR} can be described as

$$K_{UHCR} = K_N \cdot Q_N \cdot v_{o\alpha\beta,f}^- + K_H \cdot D \cdot \sum_{h=-5,7,-11,13} v_{o\alpha\beta,h}^\pm \quad (16)$$

where the coefficients K_N and K_H are designed to ensure that the voltage unbalance and harmonics are compensated to an

acceptable level without violating the system stability. With the UHC method, the harmonic and unbalance power sharing errors can be effectively compensated. Notably, the values of the K_N and K_H should also ensure the stability of the islanded microgrid system.

A.4. Inner Voltage and Current Control Loops

The voltage loop reference signals are modified by the virtual impedance loop, which contains the VPI, VNI, and VVHI loops, as shown in Fig. 6. The output voltage of a DG unit can be derived as

$$v_{o\alpha\beta}(s) = G(s)v_{\alpha\beta}^*(s) - (G(s)Z_{v\alpha\beta}(s) + Z_{o\alpha\beta}(s))i_{o\alpha\beta} \qquad (17)$$

where $G(s)$, $Z_{v\alpha\beta}$, and $Z_{o\alpha\beta}$ are the closed-loop voltage transfer function, resistive-inductive virtual impedance, and the output impedance without virtual impedance loops, respectively. The VNI loop at fundamental frequency is only for attenuating circulating current, which can be omitted. The transfer functions in (17) are derived as

$$G(s) = \frac{G_v(s)G_i(s)G_d(s)}{LCs^2 + (Cs + G_v(s))G_i(s)G_d(s) + 1} \qquad (18)$$

$$Z_{v\alpha\beta}(s) = Z_{v\alpha\beta,f}^+(s) + Z_{v\alpha\beta,h}(s)$$
$$= \begin{bmatrix} R_{v,f}^+ & -\omega_0 L_{v,f}^+ \\ \omega_0 L_{v,f}^+ & R_{v,f}^+ \end{bmatrix} + \begin{bmatrix} R_{v,h} & h\omega_0 L_{v,h} \\ -h\omega_0 L_{v,h} & R_{v,h} \end{bmatrix} \qquad (19)$$

$$Z_{o\alpha\beta}(s) = \frac{Ls + G_i(s)}{LCs^2 + (Cs + G_v(s))G_i(s)G_d(s) + 1} \qquad (20)$$
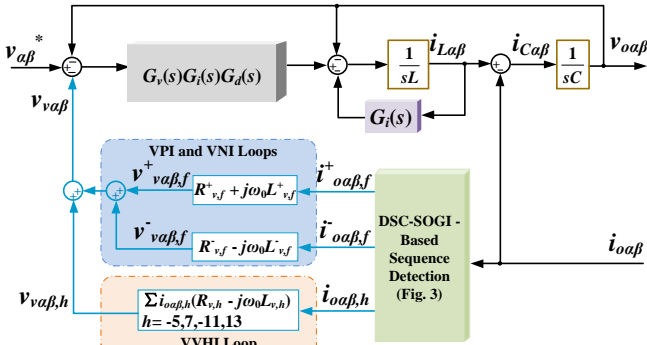
Fig. 6. Simplified diagram of the voltage and current loops integrated with virtual impedance loop.

As shown in Fig. 6, the voltage controller takes the dominant harmonic components into consideration in order to suppress output voltage harmonics. $G_i(s)$ is the proportional (k_c) current controller, and $G_v(s)$ denotes the capacitor voltage controller with a proportional and multiple resonant integral terms. $G_d(s)$ is the control delay, which includes the computational delay (T_s) and the PWM delay ($0.5T_s$).

$$G_v(s) = k_{pv} + \frac{2k_{rv}\omega_c s}{s^2 + 2\omega_c s + \omega_f^2} + \sum_{h=-5,7,-11,13} \frac{2k_{hv}\omega_c s}{s^2 + 2\omega_c s + (\omega_f h)^2} \qquad (21)$$

$$G_d(s) = \frac{1}{1 + 1.5T_s s} \qquad (22)$$

where k_{pv} is the proportional coefficients, k_{rv} is the resonant coefficients at the fundamental frequency, k_{hv} represents the coefficients of the voltage resonant controller for the hth order harmonic component, and ω_c represents cut-off frequencies of

the voltage controller, respectively.

The total output impedance with the virtual impedance loop can be derived as (23).

$$Z_{C\alpha\beta}(s) = G(s)(Z_{v\alpha\beta,f}^+(s) + Z_{v\alpha\beta,h}(s)) + Z_{o\alpha\beta}(s) \qquad (23)$$

B. The Secondary Control

In order to mitigate the problem of the inherent trade-off between power sharing and voltage and frequency regulation of the droop method, a restoration control is added to remove any steady-state error introduced by the droop controller and achieve global controllability of the microgrid that ensures nominal values of voltage amplitude and frequency under load disturbances and harmonics. The secondary control is realized by LBC link among the DG units. By using this approach, the frequency and voltage amplitude restoration compensators can be represented as

$$\omega_{sec} = k_{pf}(\omega_{MG}^* - \omega_{MG}) + k_{if}\int(\omega_{MG}^* - \omega_{MG})dt \qquad (24)$$

$$E_{sec} = k_{pe}(E_{MG}^* - E_{MG}) + k_{ie}\int(E_{MG}^* - E_{MG})dt \qquad (25)$$

where k_{pf}, k_{if}, k_{pe}, and k_{ie} are the control parameters of the proportional integral (PI) compensator of the frequency and voltage restoration control, respectively. The angular frequency levels in the microgrid (ω_{MG}) are measured and compared to the reference (ω_{MG}^*) and errors processed by the PI compensator are sent to all the DG units in order to restore the microgrid frequency. The control signal (E_{sec}) is sent to the primary control level of each DG in order to remove the steady-state errors of the droop controller.

(a)

(b)
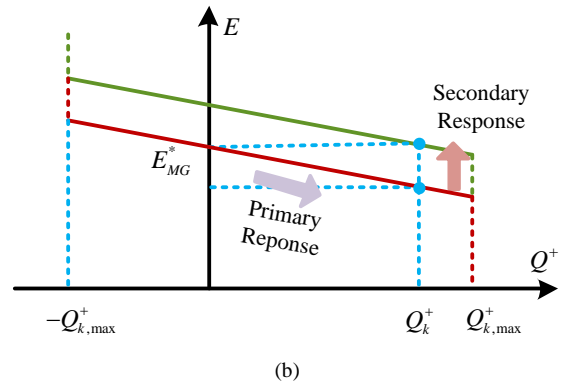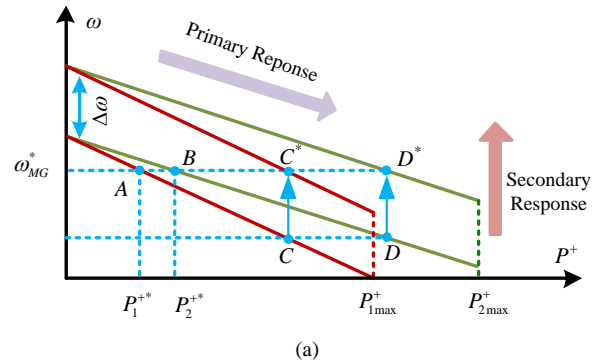
Fig. 7. Secondary control versus primary control response. (a) Frequency restoration. (b) Voltage amplitude restoration.

Fig. 7 shows the operation principle of the secondary control, which removes frequency and voltage amplitude deviation caused by primary controller. The characteristic of secondary control for frequency restoration is shown in Fig. 7(a). It can be

seen that secondary control shifts up the primary response so that frequency reaches to the nominal value. As shown in Fig. 7(a), the points of *A* and *B* are the nominal frequencies of the DG1 and DG2, respectively. The operation points of DG1 and DG2 deviate from the nominal frequencies and operate at the points of *C* and *D* when a transient increase of load is applied in the system. The idling frequency changes and the operation points of DG1 and DG2 shift to new operating points of C^* and D^* after the secondary controller is applied in the control system. Without this action, the frequency of the MG is load dependent. As shown in Fig. 7(b), the secondary control is able to remove voltage deviations caused by primary control in DG unit and the voltage amplitude restoration can be achieved.

C. The Auxiliary Control

The auxiliary control is performed selectively for the main PCC voltage harmonics [28]. Compensation reference of each harmonic ($C_{\alpha\beta}^{h\pm}$ for h^{th} voltage harmonic) is generated separately and then, all of the compensation references are added together. And the value is multiplied by the ratio of DG*i* rated power ($S_{0,i}$) and the total power of the DG units ($\sum_{j=1}^{n} S_{0,j}$) to generate the auxiliary compensation reference ($C_{\alpha\beta}^*$) which is added to the control system of Fig. 2 as a voltage reference. Fig. 8 shows the block diagram of compensation effort controller.
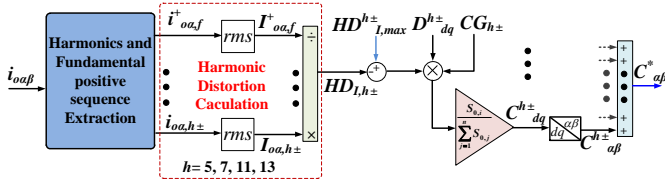
Fig. 8. Block diagram of the compensation effort controller.

According to Fig. 8, $C_{\alpha\beta}^*$ is generated as follows

$$C_{\alpha\beta}^* = \sum_{h=5,7,11,13} \left\{ (HD_{I,h\pm}^{\max} - HD_{I,h\pm}) \cdot D_{dq}^{h\pm} \cdot CG_{h\pm} \cdot \frac{S_{0,i}}{\sum_{j}^{n} S_{0,j}} \cdot \begin{bmatrix} \cos\theta & -\sin\theta \\ \sin\theta & \cos\theta \end{bmatrix} \right\}$$
(26)

where $D_{dq}^{h\pm}$ is the hth harmonic compensation for the PCC voltage in *dq* frame and $CG_{h\pm}$ is the compensation gain for the hth voltage harmonic. $CG_{h\pm}$ is a negative constant which is the same for all DGs. $HD_{I,h\pm}$ represents the hth harmonic current distortion index and $HD_{I,h\pm}^{max}$ is the maximum value of $HD_{I,h\pm}$ and the value is set to 1 when the magnitude of harmonic current remains less than the fundamental component. $S_{0,j}$ is nominal power of jth DG and *n* is the number of DGs.

V. HARDWARE-IN-THE-LOOP (HIL) RESULTS

The proposed enhanced power sharing scheme is implemented using an islanded ac microgrid consists of two parallel DG units, as shown in Fig. 9. The power stage and control parameters are given in Table I with diode rectifier load and unbalanced resistive load of a single-phase load connected to the PCC between phases *a* and *b*. The three different load conditions (unbalanced resistive load, nonlinear load, and unbalanced resistive load plus nonlinear load) are controlled by

the switch (SW) 1 and 2. The overall microgrid model is established with MATLAB/Simulink toolbox and then download into dSPACE 1006 platform based real-time digital simulator, in which the time span of the test equals to that in the real system.

TABLE I
POWER STAGE AND CONTROL PARAMETERS

System Parameter	Value
LCL filter	$L = L_o = 1.8$ mH and $C = 25$ μF
DC link voltage	650 V
Main grid	380 V (line to line *RMS*)/50Hz
Switching frequency	10kHz
DG feeder	DG1 feeder inductance and resistance $L_{DG1}=3$mH $R_{DG1}=0.2\Omega$ DG2 feeder inductance and resistance $L_{DG2}=1$mH $R_{DG2}=0.2\Omega$
Multi-loop Voltage Control Parameter	Value
k_{pv}, k_{rv}	0.175, 200
k_{hv}	50($h=-5$), 40($h=7$), 20($h=-11, 13$)
ω_c	1
k_c	5
Power Control Parameter	Value
k_p, k_q	0.0001 rad/s/W, 0.0001 V/Var
k_{pf}, k_{if}, k_{pe}, k_{ie}	0.8, 10 s^{-1}, 0.8, 10 s^{-1}
τ	50 ms
K_N and K_H	0.9, 0.4
$R_{v,f}$, $R_{v,5}$, $R_{v,7}$, $R_{v,11}$, and $R_{v,13}$	6, 1, 1, 4 and 4 Ω
$L_{v,f}$, $L_{v,5}$, $L_{v,7}$, $L_{v,11}$, and $L_{v,13}$	6, 2, 1.5, 1.5 and 1.5 mH
Load Parameter	Value
R_{UL}	230 Ω
L_{NL}, R_{NL}, C_{NL}	84 μH, 460 Ω, 235 μF

Fig. 9. Schematic of the test microgrid with two parallel-connected DG units.

To demonstrate the effectiveness of the proposed method in a microgrid with an unbalanced load, the SW1 is in the open form and the SW2 is in closed state. The sharing of load currents using the conventional droop control method is shown in Fig. 10. In the case of conventional droop control, the VHI at harmonic frequencies and VNI at fundamental frequency, the unbalance and harmonics compensation and the auxiliary control are not adopted and only the VPI at fundamental frequency is activated. Fig. 10 shows that the unbalanced load is not equally shared, and the current magnitudes of the DG1 phase *a* and phase *b* are obviously smaller than those of DG2. As the phase c of the PCC load is disconnected, it can be seen

that nontrivial circulating component appears between the phase *c* of DG1 and DG2.

When the power sharing errors are compensated using the proposed method, the output voltages and currents of DG units are given in Fig. 11. After the proposed unbalance power compensation, it can be seen that the currents of DG1 and DG2 are almost the same and the unbalance power sharing errors are effectively reduced.

(a)

(b)
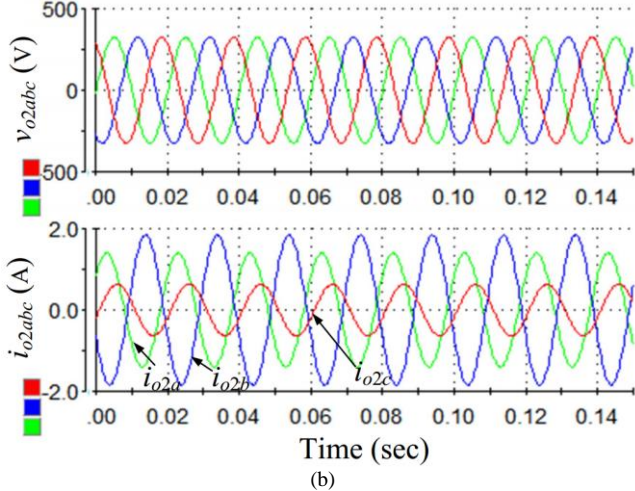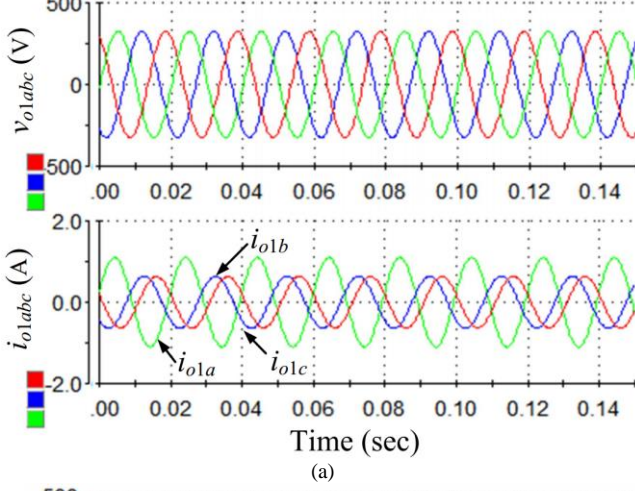
Fig. 10. Performance of the conventional droop control in a microgrid with unbalanced resistive load. (a) Output voltages and currents of DG1. (b) Output voltages and currents of DG2.

(a)

(b)
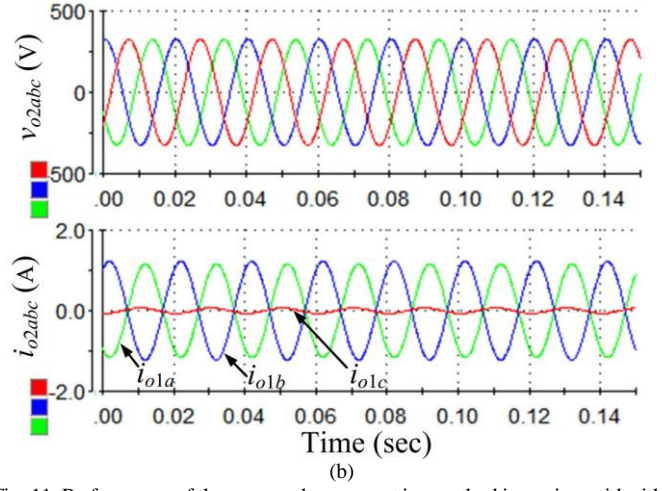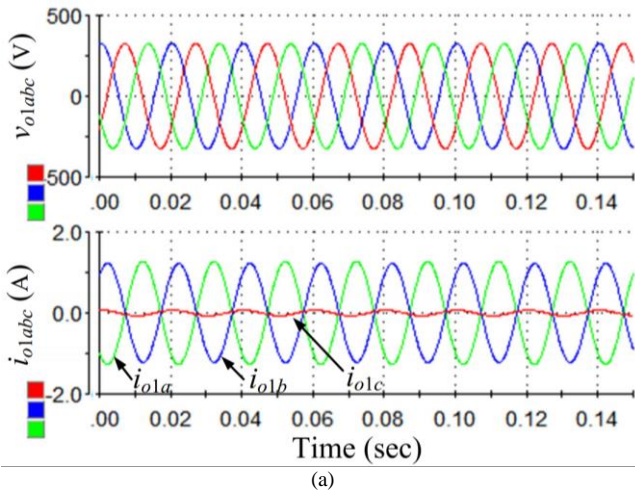
Fig. 11. Performance of the proposed compensation method in a microgrid with unbalanced resistive load with using the active damping method. (a) Output voltages and currents of DG1. (b) Output voltages and currents of DG2.

(a)

(b)
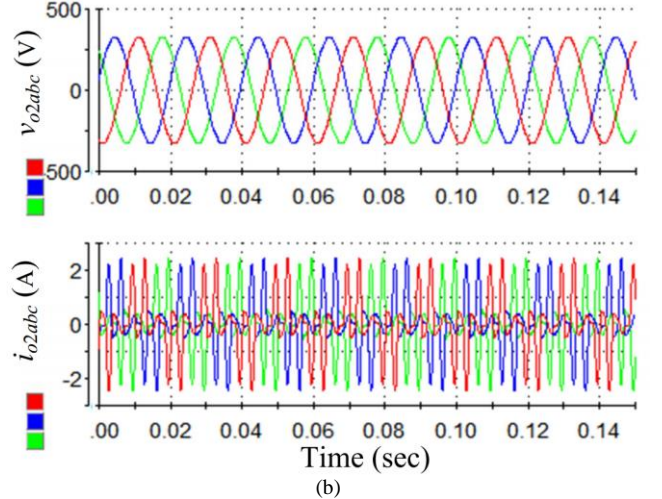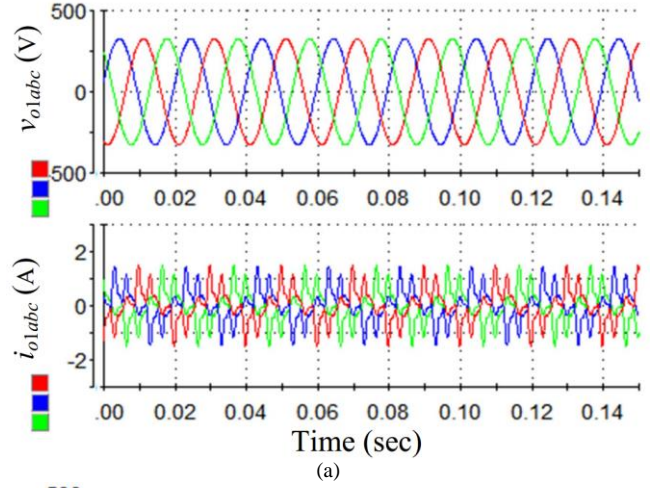
Fig. 12. Performance of the conventional droop control in a microgrid with nonlinear load. (a) Output voltages and currents of DG1. (b) Output voltages and currents of DG2.

In the case of a three-phase diode rectifier load connected to the PCC, the sharing of the harmonic load is also tested and the SW1 is in closed form and the SW2 is in open state. Fig. 12 shows the performance of the microgrid when the control of the VVHI, the harmonics compensation and the auxiliary control

are not activated. It is shown that the currents of DG1 and DG2 are not identical, and DG2 provides higher harmonic currents due to a smaller series feeder impedance. When the harmonic power sharing errors are compensated by using the proposed method, the improved power sharing performance under nonlinear loads are given in Fig. 13. It is clearly shown that the current sharing errors are effectively reduced and DG1 and DG2 have similar currents.
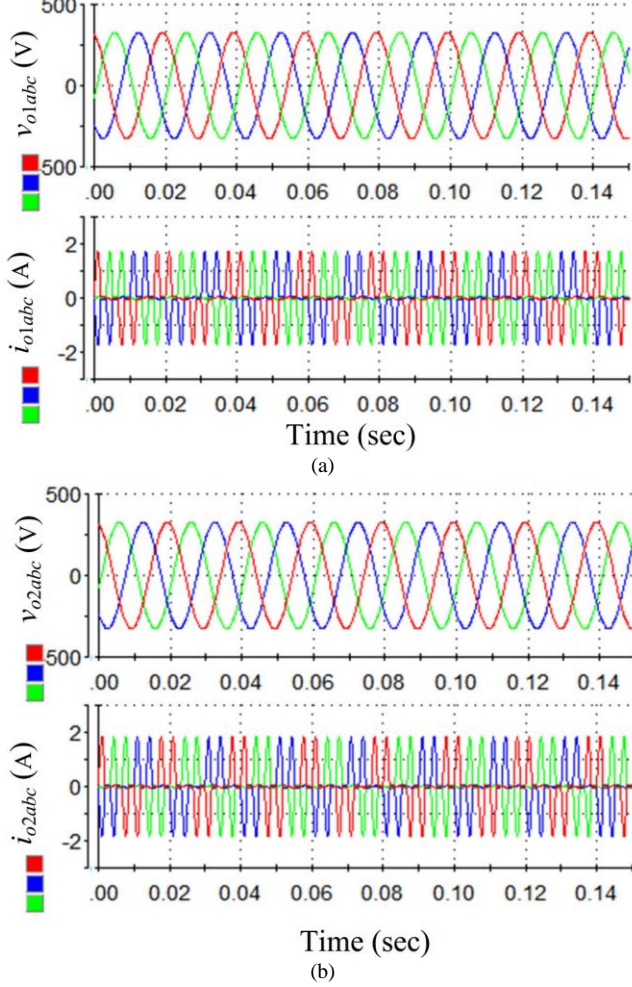
Fig. 13. Performance of the proposed compensation method in a microgrid with nonlinear load. (a) Output voltages and currents of DG1. (b) Output voltages and currents of DG2.
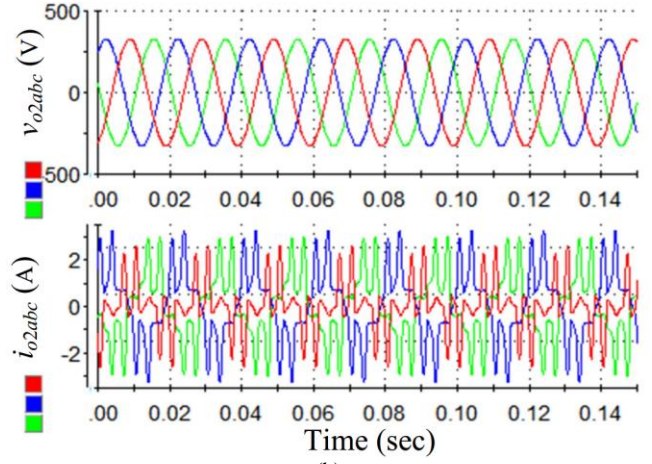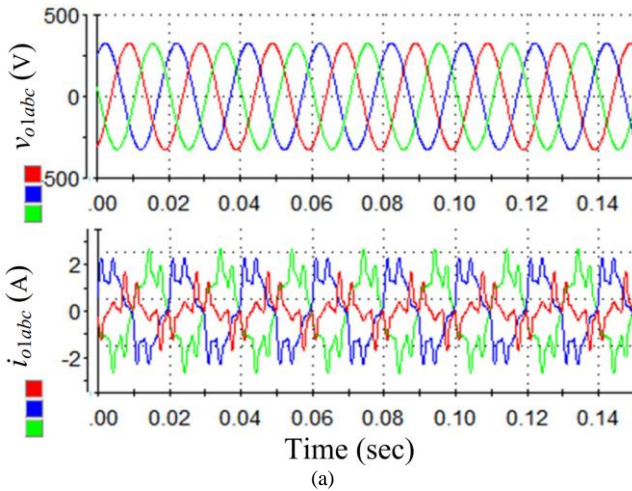
Fig. 14. Performance of the conventional droop control method in a microgrid with unbalanced resistive load plus nonlinear load. (a) Output voltages and currents of DG1. (b) Output voltages and currents of DG2.
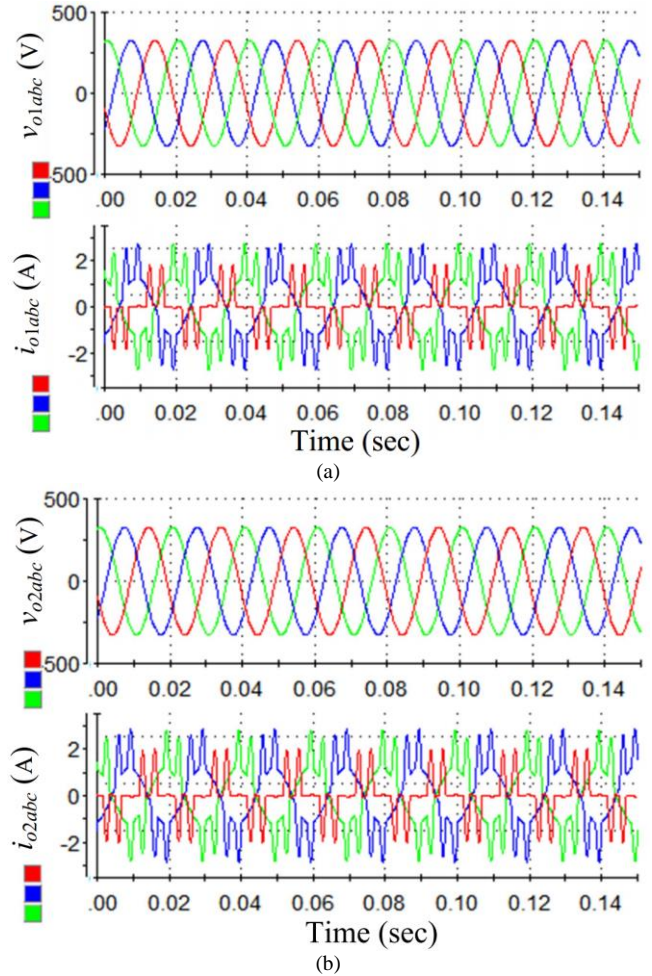
Fig. 15. Performance of the proposed compensation method in a microgrid with unbalanced resistive load plus nonlinear load. (a) Output voltages and currents of DG1. (b) Output voltages and currents of DG2.

To demonstrate the effectiveness of the proposed method in a microgrid with unbalanced resistive load plus nonlinear load connected to the PCC, the output voltages and currents of DG1 and DG2 are shown in Fig. 14 and 15 and the SW1 and SW2 are in the closed state. The load sharing performance using only conventional droop control method is depicted in Fig. 14. It is

obvious that DG2 shares a higher portion of load currents due to a smaller feeder impedance. There are some circulating currents between two DG units and the reactive, harmonic, and unbalance power sharing errors are followed by the conventional droop control. In order to reduce the microgrid power sharing errors, the proposed compensation method with the sequence of reactive power compensation, unbalance power compensation, and harmonic power compensation are adopted in the whole control system. After the activation of the proposed compensation method, the voltage and current waveforms of DG1 and DG2 are shown in Fig. 15. Compared to the simulated performance in Fig. 14, Fig. 15 demonstrates that the current sharing errors are effectively reduced and DG1 and DG2 have similar currents. It can be derived that the proposed compensation method is effective to reduce the power sharing errors in a microgrid under unbalanced resistive load and nonlinear load condition.

The performance of the secondary control strategy applied to a microgrid have been depicted in Fig. 16 and 17, respectively. Fig. 16 shows the simulation results of the proposed compensation method in a microgrid without using the secondary controller under the unbalanced and nonlinear load conditions. A 230Ω three-phase resistive load is suddenly applied at t=1s and the DG1 is disconnected at t=2s. As depicted in Fig. 16(a), the voltages of DG1 and DG2 are not exactly the same under normal operation scenario, and small deviation is observed. When DG1 is swithed off at t=2s, the voltage of DG2 drops due an increase of load. As shown in Fig. 16(b), the frequency is deviated from 50Hz, i.e., a steady-state error about 0.01Hz can be observed under normal operation scenario. With an increase of load, the frequencies of both DG1 and DG2 drop for about 0.02Hz. After the tripping of DG1, the frequency of the microgrid drops for 0.036Hz to reach a steady state of 49.964 Hz.
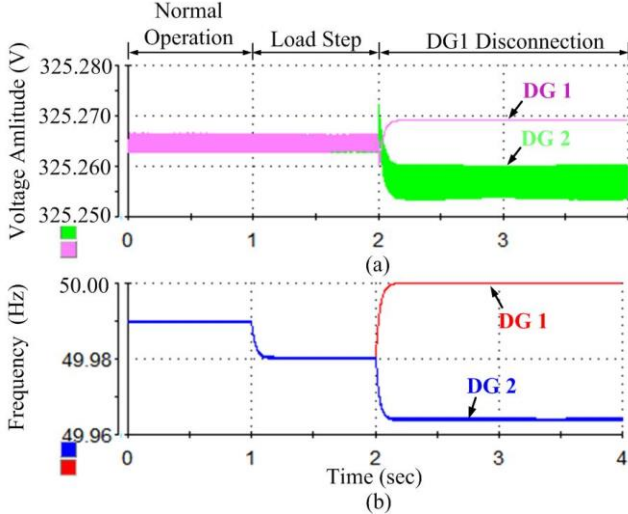
Fig. 16. Performance of the proposed compensation method in a microgrid without using secondary controller under unbalanced and nonlinear loads. (a) Voltage amplitude. (b) Frequency.

The effect of the secondary control strategy to restore the voltage and frequency deviations of the DG units with the proposed compensation strategy under the unbalanced and nonlinear load conditions is depicted in Fig. 17. It can be seen that voltage and frequency values are quickly and sucessfully

regulated inside the islanded microgrid, removing the static deviations produced by the droop control. Moreover, the secondary control restores the voltage and frequency successfully even after disconnection of one unit from the islanded microgrid.
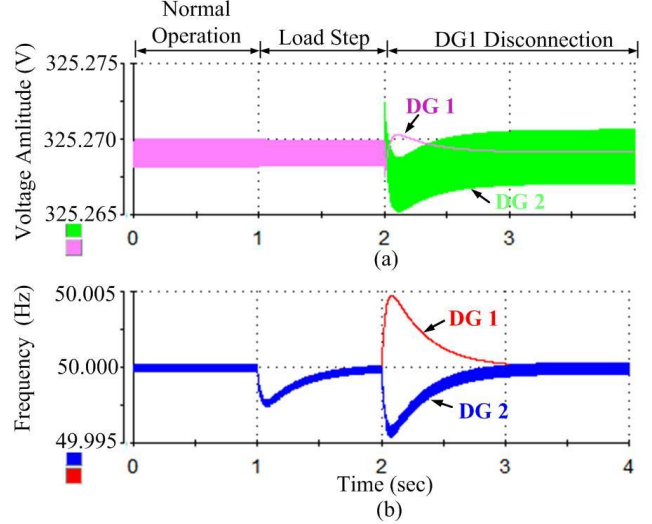
Fig. 17. Performance of the proposed compensation method in a microgrid with using secondary controller under unbalanced and nonlinear loads. (a) Voltage amplitude. (b) Frequency.
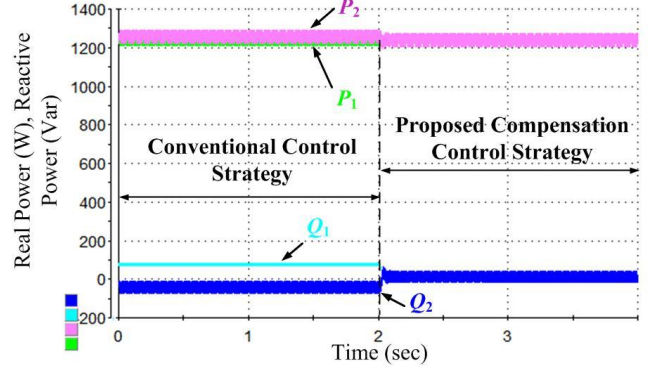
Fig. 18. Power sharing performance in a microgrid under unbalanced and nonlinear load conditions.

To further verify the effectiveness of the proposed power sharing enhancement method under the unbalanced and nonlinear load conditions, the corresponding power sharing performance are presented in Fig. 18. As shown in Fig. 18, when the conventional droop control without using unbalance and harmonics compensation, VNI and VVHI, and the auxiliary control in the control system, the real power sharing is accurate while the reactive, unbalance, and the harmonic power sharing appear as nontrivial errors. On the other hand, the reactive, unbalance, and the harmonic power sharing errors can be reduced significantly by the proposed compensation method at t=2s.

VI. CONCLUSION

This paper proposes an enhanced power sharing scheme for voltage unbalance and harmonics compensation in an islanded microgrid. The proposed method utilizes the selective virtual impedance loop, the local voltage unbalance and harmonics compensation block, and the auxiliary selective compensation of PCC voltage characteristic harmonics in a microgrid to

compensate the reactive, unbalance, and the harmonic power sharing errors. In the primary control, the selective virtual impedance at the fundamental positive sequence, fundamental negative sequence, and harmonic frequencies are adopted to enhance the power sharing of reactive, unbalance and harmonic power between the DG units. And the DSC-SOGI-based sequence decomposition method is utilized for individual harmonic component extraction, which is composed of the VPI, VNI, and VVHI. The fundamental positive-sequence real and reactive powers are used by the power controllers to generate the references of the DG output voltage amplitude and phase angle. The negative sequence and harmonic powers are applied for the generation of voltage unbalance and harmonics compensation reference signals.

Moreover, the voltage amplitude and frequency restorations are achieved by the centralized secondary controller. The auxiliary harmonic compensation is realized by the selective compensation of the characteristic harmonics of the PCC voltage. And both of them use the LBC link to produce an appropriate control signal of the central controller for the local primary controller. The hardware-in-the-loop (HIL) results of the enhanced power sharing scheme under unbalanced and nonlinear load conditions using dSPACE 1006 platform are given to demonstrate the effectiveness of the enhanced power sharing schemes.

REFERENCES

[1] F. Blaabjerg, R. Teodorescu, M. Liserre, and V. A. Timbus, "Overview of control and grid synchronization for distributed power generation systems," *IEEE Trans. Ind. Electron.*, vol. 53, no. 5, pp. 1398–1409, Oct. 2006.

[2] H. Han, X. Hou, J. Yang, J. Wu, M. Su, and J. M. Guerrero, "Review of power sharing control strategies for islanding operation of AC microgrids," *IEEE Trans. Smart Grid*, vol. 7, no. 1, pp. 200-215, Jan. 2016.

[3] J. M. Guerrero, J. C. Vasquez, J. Matas, M. Castilla, L. G. D. Vicuña, and M. Castilla, "Hierarchical control of droop-controlled AC and DC microgrids-A general approach toward standardization," *IEEE Trans. Ind. Electron.*, vol. 58, no. 1, pp. 158-172, Jan. 2011.

[4] Y. Han, P. Shen, X. Zhao, and J. M. Guerrero, "Control strategies for islanded microgrid using enhanced hierarchical control structure with multiple current-loop damping schemes," *IEEE Trans. Smart Grid*, DOI. 10.1109/TSG. 2015. 2477698.

[5] Q. Shafiee, J. M. Guerrero, and J. C. Vasquez, "Distributed secondary control for islanded microgrids-A novel approach," *IEEE Trans. Power Electron.*, vol. 29, no. 2, pp. 1018-1031, Feb. 2014.

[6] H. Mahmood, D. Michaelson, and J. Jiang, "Accurate reactive power sharing in an islanded microgrid using adaptive virtual impedances," *IEEE Trans. Power Electron.*, vol. 30, no. 3, pp. 1605-1617, Mar. 2015.

[7] I. U. Nutkani, P. C. Loh, and F. Blaabjerg, "Droop scheme with considering of operating cost," *IEEE Trans. Power Electron.*, vol. 29, no. 3, pp. 1047–1052, Mar. 2014.

[8] D. De and V. Ramanarayanan, "Decentralized parallel operation of inverters sharing unbalanced and nonlinear loads," *IEEE Trans. Power Electron.*, vol. 25, no. 12, pp. 3015–3025, Dec. 2010.

[9] Y. W. Li and C. N. Kao, "An accurate power control strategy for power electronics-interfaced distributed generation units operating in a low-voltage multibus microgrid," *IEEE Trans. Power Electron.*, vol. 24, no. 2, pp. 2977–2988, Dec. 2009.

[10] C. N. Rowe, T. J. Summers, R. E. Betz, D. J. Cornforth, and T. G. Moore, "Arctan power–frequency droop for improved microgrid stability," *IEEE Trans. Power Electron.*, vol. 28, no. 8, pp. 3747–3759, Aug. 2013.

[11] R. H. Lasseter, J. H. Eto, B. Schenkman, J. Stevens, H. Vollkommer, D. Klapp, E. Linton, H. Hurtado, and J.Roy, "CERTS microgrid laboratory test bed," *IEEE Trans. Power Del.*, vol. 26, no. 1, pp. 325–332, Jan. 2011.

[12] Q. Shafiee, J. M. Guerrero, and J. C. Vasquez, "Distributed secondary control for islanded microgrids-A novel approach", *IEEE Trans. Power Electron.*, vol. 29, no. 2, pp. 1018-1031, Feb. 2014.

[13] K. D. Brabandere, B. Bolsens, J. V. D. Keybus, A. Woyte, J. Driesen, and R. Belmans, "A voltage and frequency droop control method for parallel inverters," *IEEE Trans. Power Electron.*, vol. 22, no. 7, pp. 1107–1115, Jul. 2007.

[14] Y. Li and Y. W. Li, "Power management of inverter interfaced autonomous microgrid based on virtual frequency-voltage frame," *IEEE Trans. Smart Grid*, vol. 2, no. 3, pp. 30–40, Mar. 2011.

[15] Q. Liu, Y. Tao, X. Liu, Y. Deng, and X. He, "Voltage unbalance and harmonics compensation for islanded microgrid inverters," *IET Power Electro*., vol. 7, no. 5, pp. 1055–1063, May. 2014.

[16] J. C. Vasquez, J. M. Guerrero, M. Savaghebi, J. Eloy-Garcia, and R. Teodorescu, "Modeling, analysis, and design of stationary reference frame droop-controlled parallel three-phase voltage source inverters," *IEEE Trans. Ind. Electron.*, vol. 60, no. 4, pp. 1271-1280, Apr. 2013.

[17] M. Savaghebi, A. Jalilian, J. C. Vasquez, and J. M. Guerrero, "Autonomous voltage unbalance compensation in an islanded droop-controlled microgrid," *IEEE Trans. Ind. Electron.*, vol. 60, no. 4, pp. 1390-1402, Apr. 2013.

[18] Y. Tao, Q. Liu, Y. Deng, X. Liu, and X. He, "Analysis and mitigation of inverter output impedance impacts for distributed energy resource interface," *IEEE Trans. Power Electron.*, vol. 30, no. 7, pp. 3563-3576, Jul. 2015.

[19] M. Savaghebi, A. Jalilian, J. C. Vasquez, and J. M. Guerrero, "Secondary control scheme for voltage unbalance compensation in an islanded droop controlled microgrid," *IEEE Trans. Smart Grid*, vol. 3, no. 99, pp. 1–11, 2011.

[20] M. Savaghebi, A. Jalilian, J. C. Vasquez, and J. M. Guerrero, "Secondary control for voltage quality enhancement in microgrids," *IEEE Trans. Smart Grid*, vol. 3, no. 4, pp. 1893–1902, Dec. 2012.

[21] Q-C. Zhong, "Harmonic droop controller to reduce the voltage harmonics of inverters," *IEEE Trans. Ind. Electron.*, vol. 60, no. 3, pp. 936–945, Mar. 2013.

[22] J. He, Y. W. Li, and F. Blaabjerg, "An enhanced islanding microgrid reactive power, imbalance power, and harmonic power sharing scheme," *IEEE Trans. Power Electron.*, vol. 30, no. 6, pp. 3389-3401, Jun. 2015.

[23] X. Wang, F. Blaabjerg, and Z. Chen, "Autonomous control of inverter-interfaced distributed generation units for harmonic current filtering and resonance damping in an islanded microgrid," *IEEE Trans. Ind. Appl.*, vol. 50, no. 1, pp. 452-461, Jan./Feb.2014.

[24] N. Pogaku, M. Prodanović, and T. C. Green, "Modeling, analysis and testing of autonomous operation of an inverter-based microgrid," *IEEE Trans. Power Electron.*, vol. 22, no. 2, pp. 613-625, Mar. 2007.

[25] M. S. Hamad, M. I. Masoud, and B. W. Williams, "Medium-voltage 12-pulse converter: output voltage harmonic compensation using a series APF," *IEEE Trans. Ind. Electron.*, vol. 61, no. 1, pp. 43–52, Jan. 2014.

[26] Y. Han, L. Xu, M. M. Khan, C. Chen, G. Yao, and L. D. Zhou, "Robust deadbeat control scheme for a hybrid APF with resetting filter and ADALINE-based harmonic estimation algorithm," *IEEE Trans. Ind. Electron.*, vol. 58, no. 9, pp. 3893-3904, Sep. 2011.

[27] M. Hamzeh, H. Karimi, and H. Mokhtari, "Harmonic and negative-sequence current control in an islanded multi-bus MV microgrid," *IEEE Trans. Smart Grid.*, vol. 5, no. 1, pp. 167-176, Jan. 2014.

[28] M. Savaghebi, J. C. Vasquez, A. Jalilian, J. M. Guerrero, and T. L. Lee, "Selective compensation of voltage harmonics in grid-connected microgrids," *Mathematics and Computers in Simulation*, vol. 9, pp. 211-228, May. 2013.

[29] D. Wu, F. Tang, T. Dragicevic, J. C. Vasquez, and J. M. Guerrero, "Autonomous active power control for islanded ac microgrids with photovoltaic generation and energy storage system," *IEEE Trans. Energy Convers.*, vol. 29, no. 4, pp. 882-892, Dec. 2014.

[30] Y. Wang, Z. Chen, X. Wang, Y. Tian, Y. Tan, and C. Yang, "An estimator-based distributed voltage-predictive control strategy for ac islanded microgrids," *IEEE Trans. Power Electron.*, vol. 30, no. 7, pp. 3934-3951, Jul. 2015.

[31] A. Kahrobaeian, and Y. A. –R. Ibrahim Mohamed, "Networked-based hybrid distributed power sharing and control for islanded microgrid systems," *IEEE Trans. Power Electron.*, vol. 30, no. 2, pp. 603-617, Feb. 2015.

[32] S. J. Ahn, J. W. Park, I. Y. Chung, S. I. Moon, S. H. Kang, and S. R. Nam, "Power-sharing method of multiple distributed generators considering

control modes and configurations of a microgrid," *IEEE Trans. Power. Del.*, vol. 25, no. 3, pp. 2007–2016, Jul. 2010.

[33] H. Han, Y. Liu, Y. Sun, M. Su, and J. M. Guerrero, "An improved droop control strategy for reactive power sharing in islanded microgrid," *IEEE Trans. Power Electron.*, vol. 30, no. 6, pp. 3133-3141, Jun. 2015.

[34] A. Milczarek, M. Malinowski, and J. M. Guerrero, "Reactive power management in islanded microgrid-proportional power sharing in hierarchical droop control," *IEEE Trans. Smart Grid.*, vol. 6, no. 4, pp. 1631-1638, Jul. 2015.

[35] J. W. Jung, T. T. Vu, Q. D. Dong, T. D. Do, Y. S. Choi, and H. C. Han, "A three-phase inverter for a standalone distributed generation system: adaptive voltage control design and stability analysis," *IEEE Trans. Energy Convers.*, vol. 29, no. 1, pp. 46-56, Mar. 2014.

[36] M. N. Marwali, and A. Keyhani, "Control of distributed generation systems-part i: voltages and currents control," *IEEE Trans. Power Electron.*, vol. 19, no. 6, pp. 1541-1550, Nov. 2004.

[37] P. Rodr´ıguez, A. Luna, I. Candlea, R. Mujal, R. Teodorescu, and F. Blaabjerg, "Multiresonant frequency-locked loop for grid synchronization of power converters under distorted grid conditions," *IEEE Trans. Ind. Electron.*, vol. 58, no. 1, pp. 127–138, Jan. 2011.

[38] *IEEE standard definitions for the measurement of electric power qualities under sinusoidal, nonsinusoidal, balanced, or unbalanced conditions*, IEEE Std. 1459, 2010.

[39] H. J. Avelar, W. A. Parreira, J. B. Vieira, L. C. G. De Freitas, and E. A. Alves Coelho, "A state equation model of a single-phase grid-connected inverter using a droop control scheme with extra phase shift control action," *IEEE Trans. Ind. Electron.*, vol. 59, no. 3, pp. 1527-1537, Mar. 2012.

[40] J. He and Y. W. Li, "Analysis, design, and implementation of virtual impedance for power electronics interfaced distributed generation," *IEEE Trans. Ind. Appl.*, vol. 47, no. 6, pp. 2525-2538, Nov./Dec.2011.

Yang Han (S'08-M'10) was born in Chengdu, China. He received his Ph.D. in Electrical Engineering from Shanghai Jiaotong University (SJTU), Shanghai, China, in 2010. He joined the Department of Power Electronics, School of Mechatronics Engineering, University of Electronic Science and Technology of China (UESTC) in 2010, and where he has been an Associate Professor since 2013. From March 2014 to March 2015, he was a Visiting Scholar at the Department of Energy Technology, Aalborg University, Aalborg, Denmark. His research interests include AC/DC microgrids, grid-connected converters for renewable and DGs, phase-locked loop (PLL), power quality, active power filters and static synchronous compensators (STATCOMs). He has authored more than 20 ISI-indexed journal papers and one book chapter in the area of power electronics, power quality conditioners, and smart grid. He received Best Paper Awards from 2013 Annual Conference of HVDC and Power Electronics Committee of Chinese Society of Electrical Engineers (CSEE) in Chongqing, China, and the 4th International Conference on Power Quality in 2008, in Yangzhou, China. He has five issued and eight pending patents. He is an active reviewer for IEEE Transactions on Power Electronics, IEEE Transactions on Smart Grid, IEEE Transactions on Industrial Electronics, IEEE Transactions on Sustainable Energy and IEEE Transactions on Energy Conversion.

Pan Shen was born in Hefei, China in 1991. He received his B.S. in Electrical Engineering and Automation from Anhui Agricultural University, Hefei, China, in 2013. He is currently working toward the M.S. degree in Power Electronics and Electric Drives at the University of Electronic Science and Technology of China (UESTC), Chengdu, China. His current research interests include ac/dc microgrid, power quality, power converters, power system automation, and active power filters.

Xin Zhao received the B.S. and M.S. degree in Power Electronics & Electrical Drives from Northwestern Polytechnical University, Xi'an, China, in 2010 and 2013, respectively. He is currently working toward the Ph.D. degree at Department of Energy Technology, Aalborg University, Denmark. His research interests include control of power converters, power quality and microgrids.

Josep M. Guerrero (S'01-M'04-SM'08-FM'15) received the B.S. degree in telecommunications engineering, the M.S. degree in electronics engineering, and the Ph.D. degree in power electronics from the Technical University of Catalonia, Barcelona, in 1997, 2000 and 2003, respectively. Since 2011, he has been a Full Professor with the Department of Energy Technology, Aalborg University, Denmark, where he is responsible for the Microgrid Research Program. From 2012 he is a guest Professor at the Chinese Academy of Science and the Nanjing University of Aeronautics and Astronautics; from 2014 he is chair Professor in Shandong University; from 2015 he is a distinguished guest Professor in Hunan University; and from 2016 he is a visiting professor fellow at Aston University, UK.

His research interests is oriented to different microgrid aspects, including power electronics, distributed energy-storage systems, hierarchical and cooperative control, energy management systems, smart metering and the internet of things for AC/DC microgrid clusters and islanded minigrids; recently specially focused on maritime microgrids for electrical ships, vessels, ferries and seaports. Prof. Guerrero is an Associate Editor for the IEEE TRANSACTIONS ON POWER ELECTRONICS, the IEEE TRANSACTIONS ON INDUSTRIAL ELECTRONICS, and the IEEE Industrial Electronics Magazine, and an Editor for the IEEE TRANSACTIONS on SMART GRID and IEEE TRANSACTIONS on ENERGY CONVERSION. He has been Guest Editor of the IEEE TRANSACTIONS ON POWER ELECTRONICS Special Issues: Power Electronics for Wind Energy Conversion and Power Electronics for Microgrids; the IEEE TRANSACTIONS ON INDUSTRIAL ELECTRONICS Special Sections: Uninterruptible Power Supplies systems, Renewable Energy Systems, Distributed Generation and Microgrids, and Industrial Applications and Implementation Issues of the Kalman Filter; the IEEE TRANSACTIONS on SMART GRID Special Issues: Smart DC Distribution Systems and Power Quality in Smart Grids; the IEEE TRANSACTIONS on ENERGY CONVERSION Special Issue on Energy Conversion in Next-generation Electric Ships. He was the chair of the Renewable Energy Systems Technical Committee of the IEEE Industrial Electronics Society. He received the best paper award of the IEEE Transactions on Energy Conversion for the period 2014-2015. In 2014 and 2015 he was awarded by Thomson Reuters as Highly Cited Researcher, and in 2015 he was elevated as IEEE Fellow for his contributions on "distributed power systems and microgrids."